Celldetective: an AI-enhanced image analysis tool for unraveling dynamic cell interactions

Rémy Torro[1,2*], Beatriz Dìaz-Bello[1], Dalia El Arawi[1], Lorna Ammer[1,3], Patrick Chames[3], Kheya Sengupta[2], Laurent Limozin[1*]

[1*]Aix-Marseille Univ, CNRS, INSERM, Turing Centre for Living systems, LAI, Marseille, France.
[2]Aix-Marseille Univ, CNRS, Turing Centre for Living systems, CINAM, Marseille, France.
[3]Aix-Marseille Univ, CNRS, INSERM, Institut Paoli-Calmettes, CRCM, Marseille, France.

*Corresponding author(s). E-mail(s): remy.torro@inserm.fr; laurent.limozin@inserm.fr;

Abstract

A current key challenge in bioimaging is the analysis of multimodal and multidimensional data reporting dynamic interactions between diverse cell populations. We developed Celldetective, a software that integrates AI-based segmentation and tracking algorithms and automated signal analysis into a user-friendly graphical interface. It offers complete interactive visualization, annotation, and training capabilities. We demonstrate it by analyzing original experimental data of spreading immune effector cells as well as antibody-dependent cell cytotoxicity events using multimodal fluorescence microscopy.

Keywords: bioimage analysis, multimodal microscopy, artificial intelligence, immune cell interactions

Modern biomedical research relies on high throughput and high resolution experimental assays which require advanced and powerful analysis tools. High content, multi-channel spatio-temporal imaging of living cells is an important example. Deep learning (DL) has revolutionized this field [1, 2]. Yet, extracting scientific

insights from such complex data remains challenging, requiring coding skills [3] or proficiency in integrating/mastering disparate tools [4]. A primary step in image analysis is cell segmentation, for which DL tools are highly successful [5, 6], but rely on pretrained models for which the original dataset is not always accessible or too remote from user's data [7], preventing transfer learning. For dynamic data, the tracking of cells is also crucial [8, 9]. Currently, there are almost no solutions that integrate the two tasks [10]. Furthermore, single-cell image sequences contain time-dependent signals giving access to functional information, traditionally collected or treated manually [11, 12]. Existing softwares, though sometimes capable of measuring features [13], are not conceived for dynamic signals, nor linked to DL based event-detection. Here, we introduce Celldetective, an open-source Python-based solution with a graphical user interface (GUI) for annotation and dynamic analysis of 2D multimodal time-lapse microscopy sequences from mixed cell populations. Celldetective incorporates advanced functionalities such as state-of-the art segmentation, tracking, signal-analysis, event-detection, and cell-cell interaction analysis. The framework accommodates complete retraining within the GUI. We demonstrate the software capabilities through two applications: i) measuring immune cell decision time in a cell-surface assay using label-free microscopy and ii) measuring dynamic cell-cell interactions in a multiwell co-culture of immune and target cells, an established cytotoxic assay, using multi-color fluorescence microscopy.

Typically used for multi-dimensional images from biological samples in multi-well chambers (Fig. 1 Top and Supplementary Fig. 1), Celldetective generates quantitative output such as cell trajectories, time-dependent signals and event-detections. The analysis pipeline is shown in Fig. 1, featuring main functions of the software (left column) and data input/output (right column). For cell segmentation, generalist DL models StarDist [5] and Cellpose [6] are used and both are made available natively (Supplementary Tab. 1). However, these models exhibit limited performance when faced with a mixture of cell types with different sizes (Supplementary Fig. 2A-D) or modalities not encountered during training (Supplementary Fig. 2E-H). We therefore specifically trained models using dedicated datasets for the applications described below. The GUI emulates a napari visualization tool [4] to allow manual correction of segmentation masks (Supplementary Fig. 3). Corrected masks serve as ground truth to fine-tune the generalist DL model [4, 6] or train a specialized model from scratch (Supplementary Fig. 4). Cell tracking is performed by the Bayesian tracker btrack [8] which is fully parametrizable in the GUI, with options for adding a selection of cell features for improved performance, post-processing of tracks (Supplementary Fig. 5) and visualization via Napari. Single-cell measurements are based either on the segmentation masks, which include morphology, texture and tone, or on trajectories centered ROIs, providing continuous intensity signal measurements. Based on time-traces, single-cell event-detection can be performed by time-series analysis using a dedicated visualization and manual annotation menu (Supplementary Fig. 6). Automated classification and regression are available as a DL approach (Supplementary Fig. 7 and Tab. 4). Signal annotations can be used as training data to enhance or automatize the event-detection DL model. The tracking and measurement data can be exported as tables for each labeled cell population,

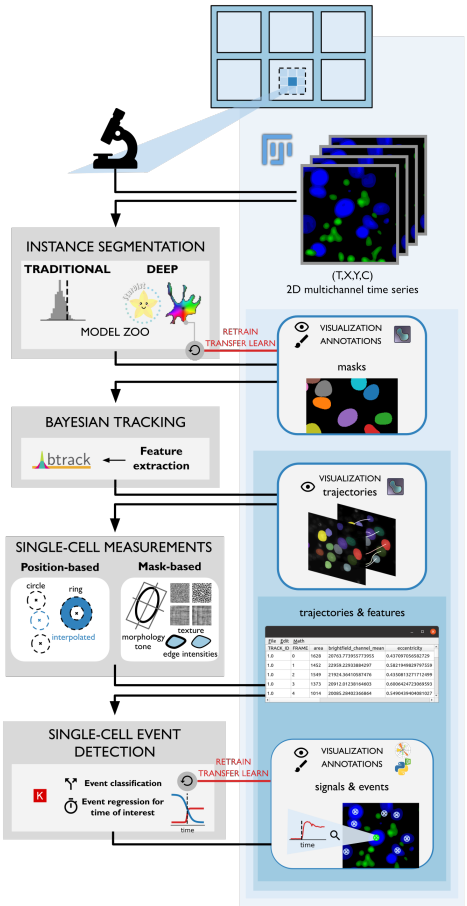

Fig. 1 Functional description of Celldetective. Multi-channel timeseries microscopy data is fed into Celldetective, in a file structure mimicking that of multi-well plates. The processing modules are shown on the left column, whereas the output and visualization modules are displayed on the right column. The pipeline features successively (from top to bottom): 1. Instance segmentation (either with traditional thresholding or Deep Learning, based on a model zoo, using StarDist [5] or Cellpose [6]). The output data are masks, which can be visualized and annotated using Napari [4], for optional retraining of the model. 2. Bayesian tracking associated with feature extraction (btrack [8]), the output data being trajectories, which can also be visualized with Napari. 3. Single cell measurements of intensity, morphology, texture (based on cell position or on mask), the output being tables of trajectories enriched with features. 4. Event-detection from single cell time signal based on DL analysis. The output are time-dependent states which can be visualized on a home-made interface, designed for further annotation. Newly annotated data can be used for model retraining and transfer learning, as indicated by red lines.

allowing further exploitation. The software is compatible with standard data formats, typically generated using acquisition plugins like micromanager [14]. Data are stored at each step of the analysis (optimized for memory usage, tested on 8 Gb movies, total experiment size up to 100 Gb). The diverse software functionalities are listed in Supplementary Tab. 5, and compared to existing software. Notably, Celldetective

stands out by offering training and transfer options in segmentation, as well as signal annotation and survival analysis. The software manual is available online. To demonstrate its capabilities, we present analysis of an original cell spreading assay and a cornerstone antibody-dependent cell cytotoxicity (ADCC) setup (Fig. 2).

In the first application, we study the dynamics of Natural Killer (NK) cells spreading on a cancer cell mimetic surface (Fig. 2A-E). A potentially therapeutic bispecific antibody (bsAb) bridges the NK cell CD16 receptors, essential for ADCC, and the surface-anchored antigen HER-2. Cell-surface contact and spreading are detected by reflection interference contrast microscopy (RICM) [4, 5]. The segmentation of the contact patch is achieved after a thresholding procedure (Supplementary Fig. 8) and manual correction (Supplementary Fig. 3). The pipeline is summarized in Supplementary Fig. 9. Tracked masks, represented by contours in Fig. 2A, enable the measurement and plotting of cell-area and their normalized intensity over time (Fig. 2B). The moment of contact (t_{contact}) and onset of spreading (t_{spread}) are determined from intensity values according to principles of RICM as the point at which intensity becomes respectively greater than and less than the background. Cell trajectories in the intensity *vs* area plane are represented as a scatter plot with the color code indicating the time counted from t_{spread} (Fig. 2C). The hovering duration, calculated for each cell as $t_{\text{spread}} - t_{\text{contact}}$ (Supplementary Fig. 10), is compiled for the whole cell population as a survival curve and reported for various bsAb concentrations (Fig. 2D). We observed significant variations in cell decision time within the 10-100 pM range of bsAb. The spreading velocity at the onset of spreading is also measured for each cell and illustrated in a scatter plot as a function of bsAb concentration (Fig. 2E). Overall, the decision time of individual cells to spread, measured at high-throughput, illustrates the capabilities of Celldetective in the context of cell-surface interactions.

In the second application, we study ADCC in a high-density co-culture of effector NK cells and target tumor cells, optionally in presence of bsFab (Fig. 2F-K). Live cell nuclei, NK cytoplasm, dying cells, and NK cells' degranulation (CD107a or LAMP-1) are labelled and imaged by fluorescence microscopy(Fig. 2F). First, in a target-centric approach, target nuclei are segmented using a customized StarDist model that detects selectively target nuclei among all nuclei (Supplementary Tab. 2) and are subsequently tracked. The pipeline is summarized in Supplementary Fig. 11. Nuclear radius and fluorescent intensity of the cell death marker are measured and plotted as a function of time (Figs. 2G and Supplementary Fig. 6). Non-dying cells show no increase in the fluorescent signal, and maintain a constant apparent nuclear area. Conversely, dying target cells display a simultaneous increase in the intensity signal and decrease in the apparent area of the nucleus. Onset of both events, determined using a trainable DL model, mark the time of cell death (Supplementary Fig. 7). The compilation of dying times for the entire cell population is then presented as a survival curve, for each different tested concentrations of bsAb (Fig. 2H). The mean death time is 63 min after putting cells in co-culture with 100 pM bsAb. Next, shifting the focus to effectors, individual NK cells are segmented using a customized Cellpose model (Supplementary Tab. 3) and tracked. Finally, the target neighborhood is configured (Supplementary Figs. 12, 13) and a significant reduction in velocity of proximal NK cells, as well as an increase in LAMP-1 signal, is observed in the presence of bsAb (Fig. 2J). To

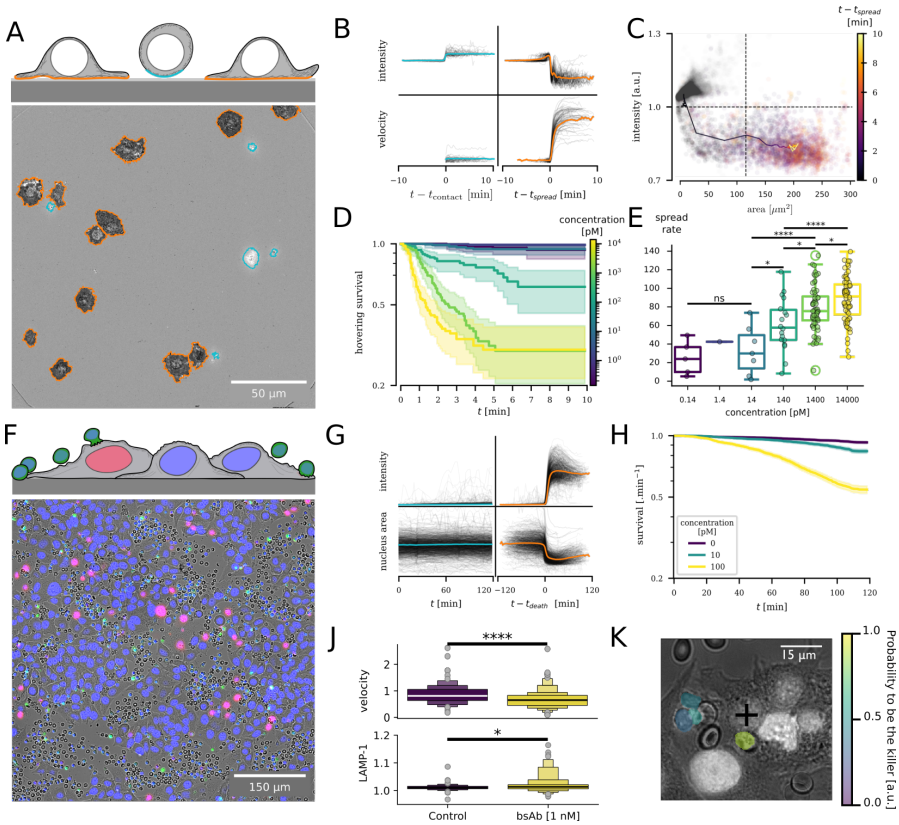

Fig. 2 Cell spreading and cytotoxicity analyzed with Celldetective. A. Top. Schematics of NK cell spreading on an antigen coated surface mediated by a bispecific antibody. Bottom. Representative normalized RICM image showing cells at different stages of spreading. Masks determined by segmentation are shown as colored contours (orange for spreading cells, blue for non-spreading cells). B. Intensity and area of contact as a function of time, for a set of non-spreading cells (left) and spreading cells (right). The reference time is the first detection $t_{contact}$ for non-spreading cells and the onset of spreading t_{spread} for spreading cells. The colored curves represent the mean of all curves. C. Intensity vs area plot for all cells at all measured points with a time color code for spreading cells. The plain line represents the average trajectory. D. Hovering survival as a function of bispecific antibody concentration (see color code). The hovering duration is defined as t_{spread}-$t_{contact}$. E. The initial spread rate (in μm^2/min) is represented as a function of bispecific antibody concentration. F. Top. Schematics of target/NK cells co-culture assay for bispecific ADCC. Bottom. Representative multimodal composite image with target nuclei labelled in blue, dying cells in red and NK cells in green. G. Intensity and nucleus apparent area for a set of non-dying target cells (left) and of dying cells (right); the reference time is the death time for the dying cells. H. Survival curve for different antibody concentrations. J. Comparison of NK cells in the neighbourhood of targets cells in the absence (Control) or presence of bispecific Ab. Top: Velocity. Bottom: Normalized Lamp-1 signal. K. Target-centered snapshot (central cross) showing the potential killer NKs with a mask whose color indicates the probability to be the killer (see Supplementary Fig. 14 for details).

identify the NK cells responsible for the death of a given tumor cell, a pair-wise probability is expressed as a linear combination of four parameters (Supplementary Tab. 6 and Fig. 14A-C). The weight for each parameter is optimized based on a

manually annotated ground truth, in order to maximize the probability of identifying the true killer. An example of prediction is shown in Supplementary Fig. 14D-E, where we achieve a prediction of the true killer in 90% of cases. These results demonstrate that the software provides an automated method to determine killer/victim pairs in a dense population of each cell type, paving the way for a detailed and high-throughput analysis of individual cell behavior and interactions.

In conclusion, Celldetective is a user-friendly software designed for non-specialists, providing advanced cell-scale analysis for large cell populations. By combining high time-resolution with robust statistical capabilities, we have uncovered new fundamental parameters characterizing dynamic interactions between immune and tumor cells. We demonstrated the efficiency of Celldetective through two applications in the context of immunotherapy by isolating time-dependent cell-scale parameters and paired-interactions, in high cell-density environment. We believe that such approach holds great potential for enhancing the design and discovery of drugs in a more powerful and rational manner, while also finding broader applications in fundamental cell biology.

Supplementary information. Supplementary methods, tables, figures and movies are available online.
Datasets and models are available at: https://zenodo.org/records/10650279.
Source code is available at: https://github.com/remyeltorro/celldetective
Software documentation is available at: https://celldetective.readthedocs.io

Author contributions. RT, BDB, LL conceived the project. PC, KS, LL supervised the project. RT designed and developed the software. RT, BDB tested the software. BDB, DEA, LA carried out experiments. PC contributed reagents. RT, BDB, DEA, LA, LL analyzed the data. RT, KS, LL wrote the manuscript. All authors critically revised the manuscript.

Acknowledgments. We thank Cristina Gonzalez and Maddy Messa N'Dong for preliminary experiments; Adrien Aimard, Dominique Touchard, Martine Biarnes and Florian Dupuy for excellent technical support; Pierre-Henri Puech and Thierry Galliano for fruitful discussions. We thank AMIDEX Emergence Innovation (project ForSelecAntibody), Plan Cancer PhysCancer program (project ComPhysAb). The project leading to this publication has received funding from France 2030, the French Government program managed by the French National Research Agency (ANR-16-CONV-0001) and from Excellence Initiative of Aix-Marseille University - A*MIDEX.

References

[1] Moen, E. *et al.* Deep learning for cellular image analysis. *Nature Methods* **16**, 1233–1246 (2019).

[2] Alieva, M., Wezenaar, A. K. L., Wehrens, E. J. & Rios, A. C. Bridging live-cell imaging and next-generation cancer treatment. *Nature Reviews Cancer* (2023).

[3] Windhager, J. *et al.* An end-to-end workflow for multiplexed image processing and analysis. *Nature Protocols* (2023).

[4] von Chamier, L. *et al.* Democratising deep learning for microscopy with ZeroCostDL4Mic. *Nature Communications* **12**, 2276 (2021).

[5] Weigert, M., Schmidt, U., Haase, R., Sugawara, K. & Myers, G. *Star-convex Polyhedra for 3D Object Detection and Segmentation in Microscopy*, 3655–3662 (IEEE, Snowmass Village, CO, USA, 2020).

[6] Pachitariu, M. & Stringer, C. Cellpose 2.0: How to train your own model. *Nature Methods* **19**, 1634–1641 (2022).

[7] Edlund, C. *et al.* LIVECell—A large-scale dataset for label-free live cell segmentation. *Nature Methods* **18**, 1038–1045 (2021).

[8] Ulicna, K., Vallardi, G., Charras, G. & Lowe, A. R. Automated deep lineage tree analysis using a Bayesian single cell tracking approach. *Frontiers in Computer Science* **3**, 734559 (2021).

[9] Ershov, D. *et al.* TrackMate 7: Integrating state-of-the-art segmentation algorithms into tracking pipelines. *Nature Methods* (2022).

[10] Padovani, F., Mairhörmann, B., Falter-Braun, P., Lengefeld, J. & Schmoller, K. M. Segmentation, tracking and cell cycle analysis of live-cell imaging data with Cell-ACDC. *BMC Biology* **20**, 174 (2022).

[11] Salles, A. *et al.* Barcoding T Cell Calcium Response Diversity with Methods for Automated and Accurate Analysis of Cell Signals (MAAACS). *PLoS Computational Biology* **9**, e1003245 (2013).

[12] Vanherberghen, B. *et al.* Classification of human natural killer cells based on migration behavior and cytotoxic response. *Blood* **121**, 1326–1334 (2013).

[13] McQuin, C. *et al.* CellProfiler 3.0: Next-generation image processing for biology. *PLOS Biology* **16**, e2005970 (2018).

[14] Edelstein, A. D. *et al.* Advanced methods of microscope control using μManager software. *Journal of Biological Methods* **1**, 10 (2014).

[15] Limozin, L. & Sengupta, K. Quantitative Reflection Interference Contrast Microscopy (RICM) in Soft Matter and Cell Adhesion. *ChemPhysChem* **10**, 2752–2768 (2009).

[16] Gonzalez, C. *et al.* Nanobody-CD16 Catch Bond Reveals NK Cell Mechanosensitivity. *Biophysical Journal* **116**, 1516–1526 (2019).

Supplementary Material

Celldetective: an AI-enhanced image analysis tool for unraveling dynamic cell interactions

Remy Torro et al.

Methods

Antibodies design and production

The bispecific antibody (bsAb) C7b-21 (or CE4-28) is a fusion of two single domain antibodies (sdAb, also called nanobodies), sdAb CE4 (or C7b) targeting against Human epidermal growth factor receptor-2 (HER-2/neu or ErbB2) [1] and sdAb C21 (or C28) targeting human CD16 (FcγRIII), using the human CH1/Ck heterodimerization motif, corresponding to the bispecific Fab (bsFab) format [2]. bsFab CE4-28 was produced by co-transfection of two plasmids using the mammalian transient system Expi293 (Thermofisher) and purified as previously described [3].

Cell lines culture, effector extraction and phenotyping

Modified MCF7-HER2+ cells were stably transfected from MCF7 cell line to overexpress HER2 receptors. Determination of HER-2 levels on the cells was performed by flow cytometry with Herceptin antibody and a secondary fluorescent anti-human antibody. Fluorescence intensity was determined and correlated with HER-2 levels. Cells were maintained in RPMI 1640 media (Gibco, Life Technologies), supplemented with 10% of Fetal Bovine Serum, FBS (Gibco, Life Technologies), 50 mg/mL of hygromycin as an antibiotic resistance selection. Cells were amplified three times per week and keep in the incubator at 37°C under 5% CO_2 atmosphere.

Primary human NK cells. NK cells were isolated as described in [4]. Briefly, blood samples were obtained from the Etablissement Francais du Sang (Marseille, France), using the MACSxpress whole-blood human NK cell isolation kit (Miltenyi Biotec, Bergisch Gladbach, Germany) a negative selection was performed. The characterization of the sorted cells was determined by flow cytometry with anti-CD16, anti-CD3 and anti-CD56 antibodies. Cells were maintained in RPMI 1640 medium and 10% FBS at 37°C, 5% CO_2 and used in the following 24 hours.

Spreading Experiment

Freshly isolated primary human NK cells were used in this experiment. A concentration of 200 000 cells/mL was added to an uncoated eight-well chambered polymer coverslip-bottom from Ibidi (80821, Ibidi, Munich). For surface preparation, the Ibidi wells were initially rinsed with PBS, followed by incubation in a solution of Biotin-labeled bovine albumin (A8549-10MG, Sigma) diluted in PBS at 100 μg/mL for 30 min at room temperature (RT) with agitation. To remove non-adsorbed BSA-biotin, the wells

were rinsed four times with PBS. Afterwards, the wells were incubated in a 10 μg/mL Neutravidin solution (31000, Thermo Scientific) diluted in PBS for 30 min at RT with agitation. After a four-time PBS wash, the wells received an Her2/ERBB2 Protein solution (10004-H27H-B, Sinobiological) diluted in 0.2% BSA at 10 nM/mL for 30 minutes at RT with agitation, followed by another four-time PBS wash. The Ibidi chamber was then placed under a microscope at 37°C. Prior to the experiment, the NK were incubated with the desired concentration of bsFab (C7b-21) during 30 min at 37°C. They were then injected in the sample. Cell spreading dynamics were observed through reflection interference contrast microscopy (RICM), a technique sensitive to cell-surface distance. The RICM setup is described in [5]. An antiflex Zeiss objective (NA = 1.25) was used with a green LED light source (λ= 546 nm) and a 14-bit CCD detector (Andor iXonEM, Oxford instruments). This configuration allows live cell observations at 37°C. Images were acquired after cell deposition in the device. To evaluate the spreading kinetics of NK cells, multiple fields of view were selected (sixteen per condition) and subjected to cyclic imaging over a 10-minute interval, facilitated by a motorized stage from Physik Instrumente, Germany. The temporal interval between successive images of a given field typically ranged from 15 to 20 seconds. An image pre-treatment, described in Supplementary Fig. 15, is applied before use of Celldetective.

ADCC Experiment

MCF7-Mod cells were used as target cells. 80 000 cells/well were seeded in an 8-well chamber μ-Slide, polymer bottom, TC treated from Ibidi (Munich, Germany). Cells were cultured overnight in RPMI complemented media and allowed to reach exponential growth (at least 18 h) under 37°C and 5% of CO_2. Next day media was aspirated and cells were incubated with Hoechst 33342 in colorless RPMI media (5 μg/mL), at 37°C during 10 min. After that, Hoechst solution were removed and the cells were rinsed 3 times with warm colorless RPMI media complemented with 10% of FBS (300 μL/well). Cells were put back in the incubator. NK primary cells were stained with CFSE dye according to the manufacturer instructions (CFSE CellTrace). 2.5 M cells were centrifuged at 1500 rpm for 5 min; the supernatant was discarded and the cells were incubated with 2.5 mL of CFSE diluted in PBS for 20 min at 37°C. After that time 12.5 mL of colorless RPMI + 10% FBS were added to the cells and incubated for 5 minutes more. Then the cells were centrifuged at 1500 rpm for 5 min. Cells were resuspended in complemented media and put back in the incubator.

Dilutions of the bsAb CE4-28 were prepared to obtain a final concentration of 1, 10 and 100 pM. The proper bsAb solution was added to each well (2 μg/mL) where the target cells were previously marked with Hoechst and incubated at 37°C during 20 min. After that time, Propidium Iodide (Sigma) was added in each well condition, then the cells were taken from the incubator and NK cells were added to each well to have a final E:T ratio of 2.5. The slide was the placed in the Zeiss AxioObserver epifluorescence microscope with temperature control at 37°C. The image acquisition consists of taking 5 to 9 fields per well, with a 20x / 0.4 objective (pixel size 0.31 μm) each field was imaged using transmitted light (Bright field), Zeiss filter set 38 (CFSE),

Zeiss filter set # 49 (Hoechst) and Zeiss filter set # 25 HE (Propidium iodide). Each position was imaged during 2-3 hours with approx. 3 min/frame

For NK tracking, the observation was realized with a 40x / 1.3 Oil Dic (UV) objective (pixel size 0.157 μm) and at 1.73 min per frame. Additionally, the NK to target ratio was set to 1:1. For monitoring degranulation, fluorescent anti-LAMP1 (Biolegend APC labelled Clone. H4A3 Cat. 328619) antibody were added at 5 μl for 1 M NK cells.

Hardware and software

Software development and analysis was carried on an Intel-core i9 CPU, NVIDIA RTX 3070 GPU, 16 Go of RAM, Ubuntu 20.04 desktop. The software was extensively tested on an Intel-core i9 CPU desktop running on Windows 11, an Intel-core i7-8565U laptop running on Windows 11, and an older Intel(R) Core(TM) i5 CPU 750 @ 2.67 GHz desktop running on Ubuntu 20.04.

The software is a python package augmented with a PyQt5 user-interface. The UI occasionally integrates Matplotlib canvases for image, animation and plot purposes. The GUI styling is based on Material Design. Each of the processing modules (segmentation, tracking, measurement, signal analysis) triggers a subprocess that applies to a single movie at a time. Upon completion of the subprocess, CPU and GPU memories are fully released, allowing to reiterate the process on the next movie or to unfreeze the GUI. Multi-threading was implemented where it is applicable and can be configured in the software.

At each module, an output (image, table) is written on the disk (in the experiment folder) and can be read as the input to the next module. This approach provides a regular and automatic saving of the data and the modularity allows flexibility in the input data that can be intuitively imported from external sources (ImageJ, Cellpose UI...). In more detail, the segmentation module outputs mask images (frame by frame). The tracking module outputs a trajectory table for the cell population of interest. The measurement and signal analysis modules build on the trajectory tables by adding columns. The neighborhood module adds columns to the trajectory tables and saves a pickle file with a nested-dictionary table with information about the neighbors at each time point.

Analysis

Signal analysis

The signals are normalized independently using user-defined choices (percentile min-max, absolute values, clipping or no clipping). Gaps in the signals are automatically interpolated. The data is split into a training, validation and test set. The signals from the training set are augmented using time shifts (translations along the time axis) to build artificially a uniform distribution of event times, eliminating bias, random signal amplification and noise.

The event detection models consist of two consecutive ResNet-like models sharing the same backbone but differing in the head and therefore the task, respectively classification and regression. The input signals are cast in a tensor of shape ($T \times$

n_{channels}) where n_{channels} is the number of coupled signals (or channels) and T an arbitrary maximum signal length, usually taken at 128 (frames). The input is first processed by a 1D convolution layer with a kernel of $(1,)$ to cast the input into 64 filters. Then the tensor is sent to two consecutive 1D-resblocks with a kernel of $(8,)$ and 64 filters, before a max pooling operation (size 2) accompanied by a doubling of the number of filters to 128. The tensor is processed by two additional 1D-resblocks before a global average pooling operation. A dense layer of 512 neurons is used to collect the convolution information. A dropout at 50 % is applied before the final layer that consists of three neurons for the classification with a softmax activation ("event", "no event" and "already happened") and 1 neuron with a linear activation for the regression (t_{event}). The models are trained for 300 and 600 epochs respectively, with the Adam optimizer and a user-controlled learning rate (typically 10^{-4}), to minimize the categorical cross-entropy for classification and mean squared error for regression. Class weights are introduced to fight class imbalance in the classification task. The batch size is also user controlled (typically set to 64 or 128 depending on the amount of signals available). Only cells belonging to the "event" class are sent to the regressor model (both in training and inference).

Area spreading rate

For each spread cell, the area is differentiated as a function of time using a sliding window of 5 frames (=1min 18s) looking 'forward'. The dA/dt at t_{spread} is reported, units=[μm^2/min], decomposed for each bispecific antibody concentration. Statistical difference is assessed using T-test for the means of two independent samples of scores between each well combinations. For readability, only some of the p-values are shown.

NK contact mean velocity

A neighborhood scheme at 120 px (18.8 μm) is performed to link target and effector detections. At each timepoint, an effector with more than one target neighbour is instantaneously classified as being "in-contact" with the targets. The NK velocity is computed per track using a centered sliding window of 3 frames (5.19 min when no gap). All NK detections not "in-contact" are filtered out. Instantaneous velocities "in-contact" are averaged per-track, yielding one estimator per cell. The distribution of this estimator is compared in the absence and presence of bispecific antibody (CE4-28). Statistical difference is assessed using T-test for the means of two independent samples of scores, yielding a p-value of 8×10^{-6} / **** or Kolmogorov-Smirnov test yielding 1.7×10^{-5} / ****.

NK contact mean LAMP-1

For the LAMP-1 signal, we measure the mean LAMP-1 intensity, relative to the background, over the NK cell mask 16. As described above, cells that are not in-contact at time t are filtered out. Since LAMP-1 can be transient, instead of averaging this quantity per trajectory, we take the maximum value per track. As above, the distribution of this estimator is compared in the absence and presence of bi-specific antibody (CE4-28). Since the difference is contained in the tail of the distribution, more than around the mean, we perform a Kolmogorov-Smirnov test, yielding a p-value of 0.01 / *.

Supplementary Tables

Table 1 Generalist models. This table lists the different generalist models (Cellpose or StarDist) which can be called natively in Celldetective. The sample images are cropped to (200 × 200) px and rescaled homogeneously to fit in the table.

name	modalities	# channels	dataset	sample image
`CP`	cytoplasm nucleus	2	Cellpose [6]	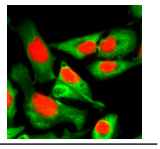
`CP_cyto`	cytoplasm nucleus	2	Cellpose [6]	/
`CP_cyto2`	cytoplasm nucleus	2	Cellpose [6] & user-submitted images	/
`CP_livecell`	cytoplasm (BF) blank	2	LiveCell [7]	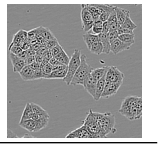
`CP_tissuenet`	cytoplasm nucleus	2	TissueNet[8]	/
`CP_nuclei`	nucleus blank	2	?	/
`SD_paper_dsb2018`	nucleus	1	subset of DSB 2018 [9]	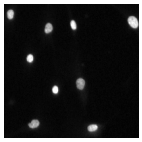
`SD_versatile_fluo`	nucleus	1	subset of DSB 2018 [9]	/
`SD_versatile_he`	H&E RGB	1	MonoNuSeg 2018 [10] TNBC 2018 [11]	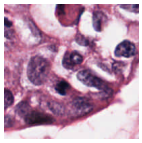

Table 2 MCF7 nuclei segmentation models in the presence of primary NK cells. Each model was trained on the same dataset of ADCC images, picking only the relevant channels.

Name	Channels	Type	Pretrained	Spatial calib. (μm)	sample image
MCF7_bf_pi_cfse_h	brightfield PI CFSE Hoechst	StarDist	None	0.3112	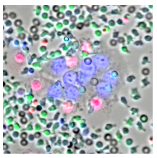
MCF7_bf_h_pi	brightfield Hoechst PI	StarDist	None	0.3112	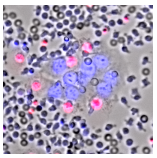
MCF7_h_pi	Hoechst PI	StarDist	None	0.3112	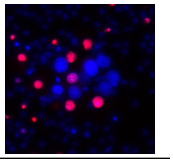
MCF7_h_versatile	Hoechst	StarDist	*versatile_fluo*	0.3112	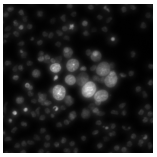

Table 3 Primary NK segmentation models. The models have been trained on a dataset of annotated primary NKs in ADCC images (*primary_NKs_w_MCF7*).

Name	Channels	Type	Pretrained	Spatial calib. (μm)	sample image
`primNK_multimodal`	brightfield CFSE Hoechst	Cellpose	None	0.2178	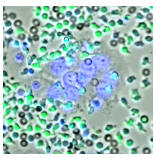
`primNK_SD`	brightfield Hoechst	StarDist	None	0.3112	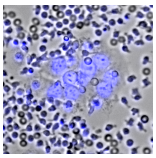
`primNK_cfse`	CFSE None	Cellpose	`CP-cyto2`	0.2178	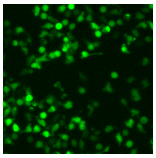

Table 4 Event detection models. We trained the following 1D DL models to classify and regress events of interest. The mean event response, centered at the event time is shown for each channel in the pattern column.

Name	Signals	Task	Pattern
lysis_H_PI	Hoechst PI	Strong PI intake	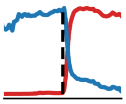
lysis_PI_area	PI area	Strong PI intake	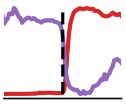
NucCond	area	Nucleus shrinking	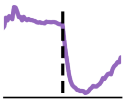

Table 5 Comparative table of software functionalities with available solutions. By convention a ✓can only be attributed if the task can be carried without coding requirement. The use of an integrated solution or plugin is indicated in parentheses.

Software feature	ImageJ/Fiji	CellProfiler	CellACDC	Celldetective
Traditional segmentation	✓	✓	✓	✓
DL segmentation	✓	✓	✓	✓
Corrections annotations	✓ (Labkit)	✓ (GIMP)	✓	✓ (napari)
Training	✗	✗	✗	✓
Transfer	✗	✗	✗	✓
Tracking	✓ (TrackMate)	✓ (TrackObjects)	✓	✓ (bTrack)
Visualization	✓ (TrackMate)	✗	✓	✓ (napari)
Position-based measurements	✓	✗	✗	✓
Measurement classification	✗	✓	✗	✓
Signal annotations	✗	✗	(✓) cell-cycle	✓
Interaction analysis	✗	✓	✗	✓
Experiment manager	✗	✗	✓	✓
Multi-condition data exploration	✗	✓ (CP Analyst)	✗	✓
Survival analysis	✗	✗	✗	✓

Table 6 Features of target/effector pairs. The table summarizes the different features considered to build the probability of finding the NK killer for the target considered. Non normalized features are activated using custom activation functions described in figure 14A-C.

Descriptor	Activation	Time-average window	Relative	Weight	Comments
d_{rel}	step function Fig. 14A	$[t_\dagger - \theta_t, t_\dagger]$	True	w_d	$d_{\text{rel}} = \sqrt{\overline{x}^2 + \overline{y}^2}$
v_{rel}	skewed function Fig. 14B	$[t_\dagger - \theta_t, t_\dagger]$	True	w_v	$v_{\text{rel}} = \frac{d}{dt} d_{\text{rel}}$ $\frac{d}{dt}$: 3-frame window bidirectional
$t^{\%}_{\text{res}}$	None	$[0, t_\dagger]$	True	w_t	$t^{\%}_{\text{res}} = \frac{t_{\in \mathcal{N}}}{t_\dagger}$
$I_{\text{LAMP-1}}$	step function Fig. 14C	$[t_\dagger - \theta_t, t_\dagger + \theta_t]$	False	w_I	Effector LAMP-1 expression

Supplementary Figures

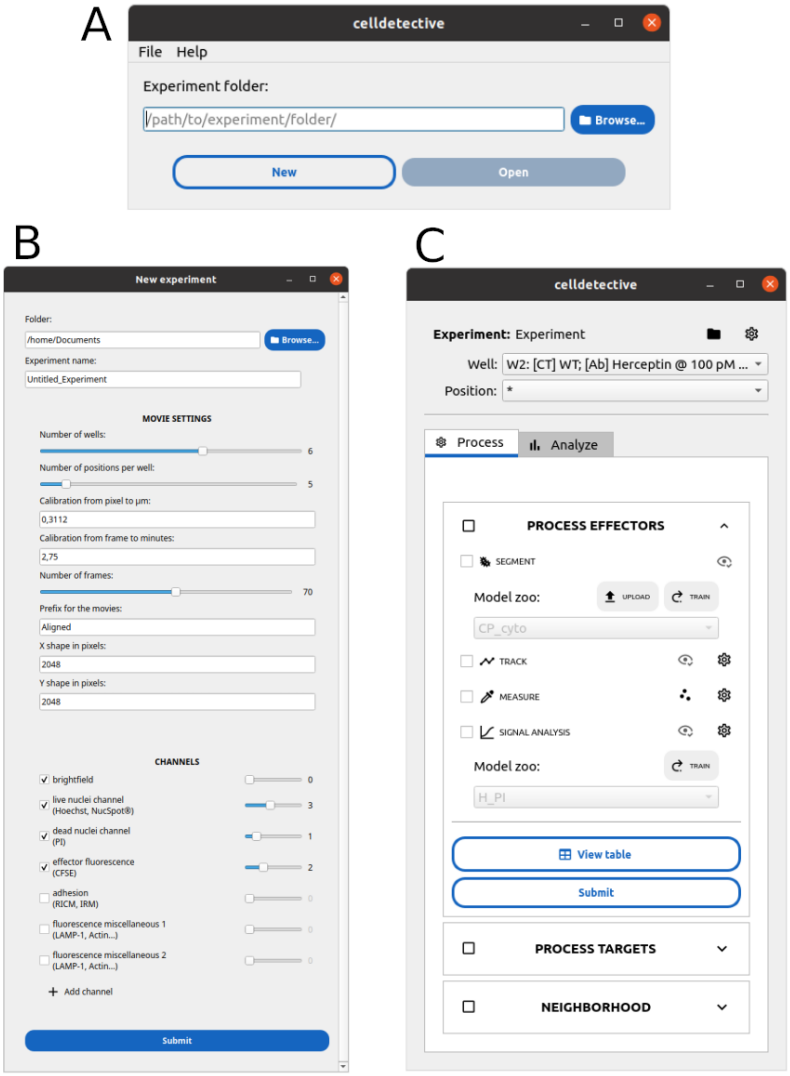

Fig. 1 Celldetective main GUI. A. Experiment selection window. B. Helper to organize a new experiment. The number of wells and number of positions per well sliders are needed to generate the folder tree. Upon clicking on the Submit button, a secondary window asks for the biological condition associated to each well. C. Main control panel allowing the analyzis of selected wells and positions. The process tab is shown, featuring processing effectors, with the 4 main steps detailed in Fig. 1.

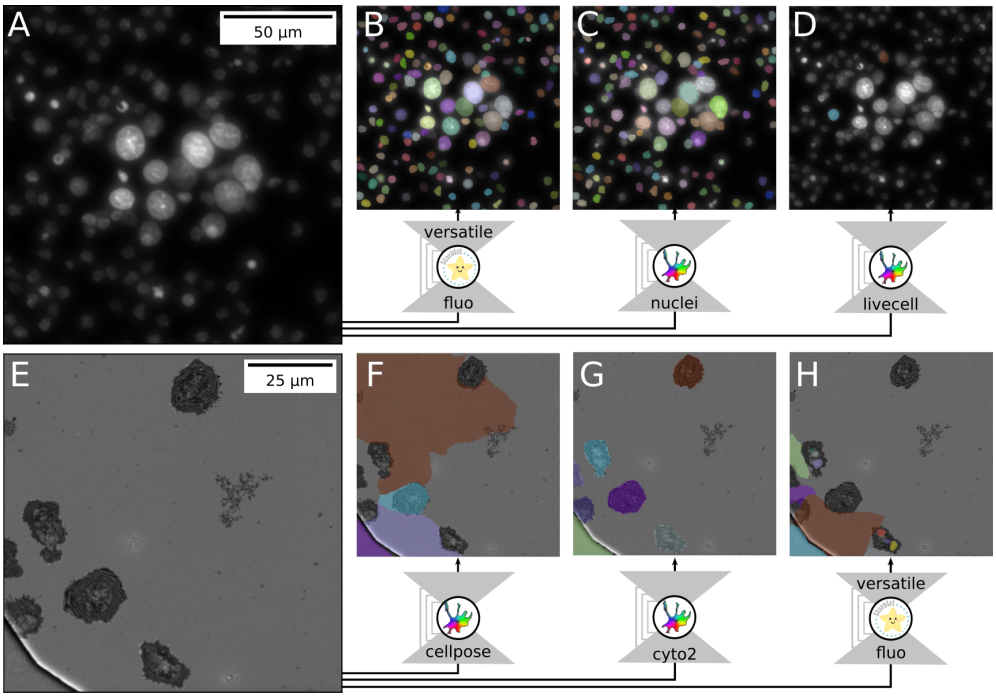

Fig. 2 Applicability of generalist models. Published generalist models (Tab. 1) can be applied to the user's microscopy data provided the images are not too different from the training set of those models. In general, these models will be non specific. A. Image of fluorescent nuclei of a mixed population of effector (human primary NK cells) and target cells (MCF7 breast cancer cells), segmented using different published models (B-D). B. StarDist *versatile fluo* model yields an excellent segmentation of both cell populations simultaneously but separating the cells in post can be a difficult process as a blurry NK nucleus is close in size to a small MCF7 nucleus. C. Cellpose *nuclei* model also achieves a high segmentation precision but the edges are pretty rough, as the images have to be considerably shrunk down before passing into the model (17 pixel nuclei). D. Cellpose *livecell* model, trained mostly on brightfield images, does not understand the nuclei data and misses most of the cells. E. RICM image of human primary NK cells spreading on a surface, segmented using different published models (F-H). F. Cellpose model misunderstands completely what a cell is in this kind of image. G. Cellpose *cyto2* model yields a very sharp segmentation of the spread cells but ignores non spread cells. It also mistakenly segments the diaphragm on at the bottom left corner of the image. H. the StarDist *versatile fluo* model is clearly a wrong model for this kind of data as the convex hypothesis is broken. Cellpose *cyto2* model is the best candidates for a transfer learning process.

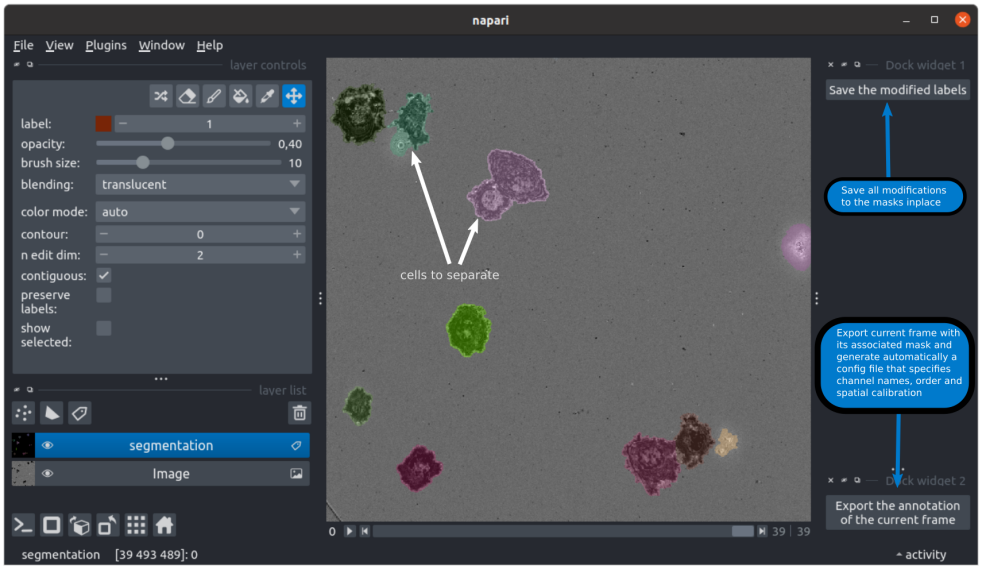

Fig. 3 Segmentation correction and annotation using Napari. Example of RICM modality with spreading NK cells. Colored masks are superimposed on the grey-scale RICM image. The user can correct the masks by painting directly on the image, for example to separate cells indicated by white arrows. New labels can be attributed and saved, the whole set of corrected masks can be exported for further tracking or retraining.

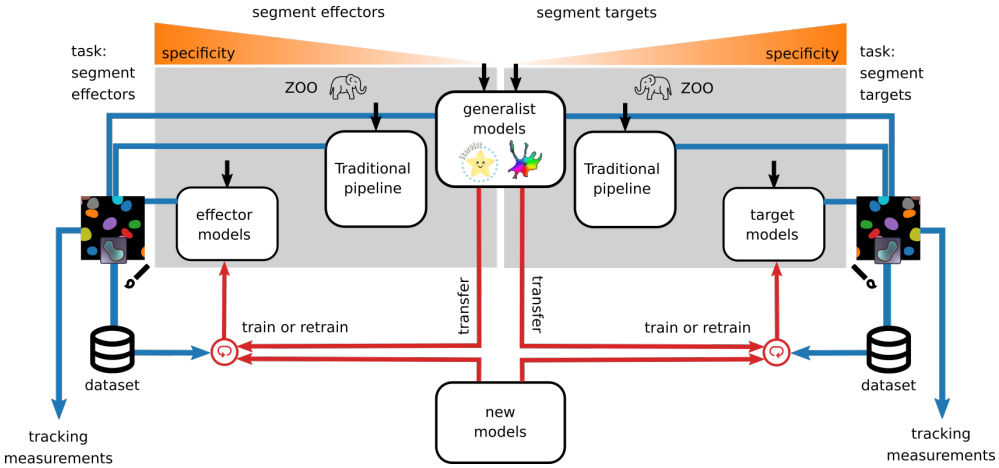

Fig. 4 Overview of segmentation options in Celldetective illustrated for a mixture of two cell populations, effector and targets. Celldetective provides several entry points (black arrows) to perform segmentation, with the intent of segmenting specifically a cell population (left: effectors, right: targets). The generalist models are listed in Tab. 1. Specific models are listed in Tab. 2 for targets and Tab. 3 for effectors. The traditional pipeline refers to a thresholding method accessible through the GUI (see Fig. 8). The masks output from each segmentation technique can be visualized and manually corrected in napari. Exporting those corrections into a dataset of paired image/masks can be used either to fit a generalist model (transfer learning) or train a new model from scratch.

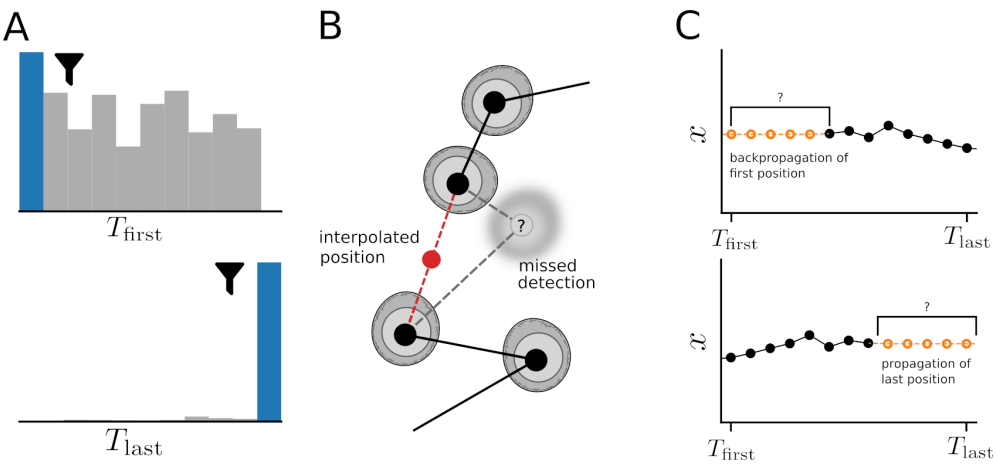

Fig. 5 Post-processing operations on trajectories. A. Endpoint filtering to remove tracks that do not start or end at the beginning and end of the movie. B. Interpolation of tracking gaps. C. Backward (resp. forward) propagation of first (resp. last) detected position to extend the time-range of the tracks.

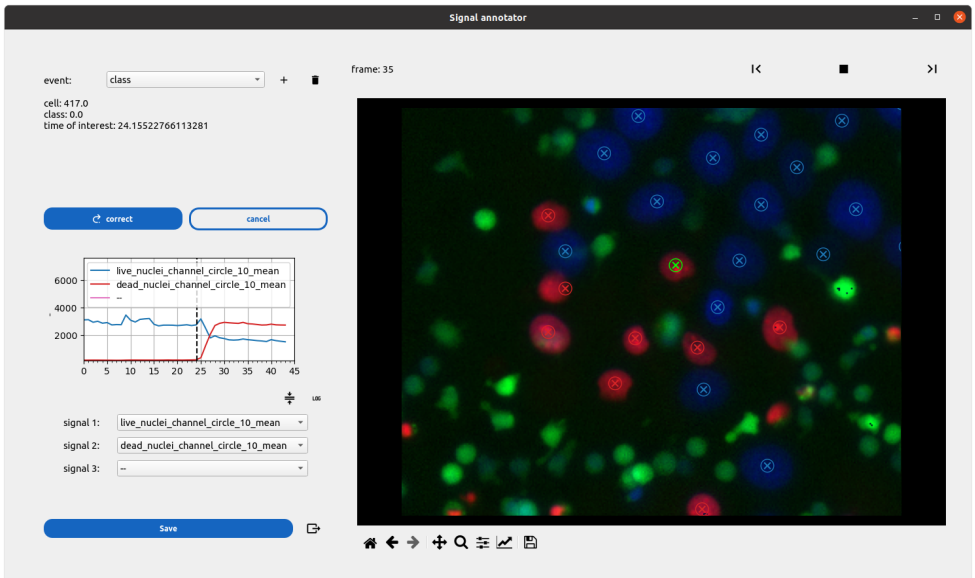

Fig. 6 Quality control on lysis detection with Celldetective, illustrated for cytotoxicity measurements. After applying the *lysis_H_PI* lysis detection model, a visual quality control is performed using Celldetective's signal annotation GUI. The image is part of a RGB composite sequence of 3 fluorescence channels (PI-red, CFSE-green and Hoechst-blue channels). The position-based intensity signal vs time is represented for the selected cell on the left graph for PI channel (red) and Hoechst channel (blue). The black vertical dotted line shows the death time t_{death} estimated by the DL model. This value can be manually corrected.

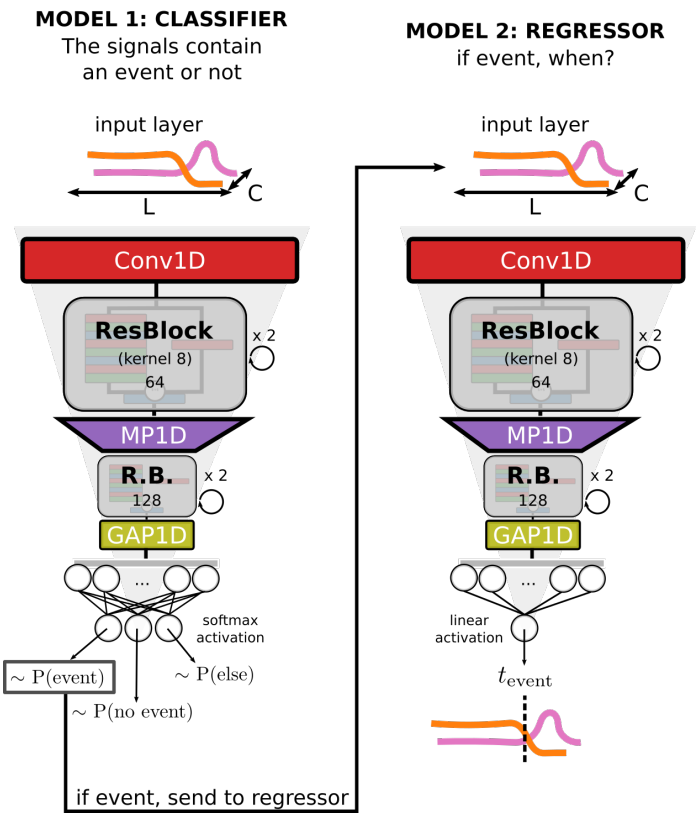

Fig. 7 Event detection by DL. The detection of a coordinated change in two fluorescence signals (Intensity vs time) is performed in parallel by a classifier and a regressor. In this example for cytotoxicity, the classifier indicates the probability of a death ocurring during the observation of the signals, while the regressor indicates the date of death.

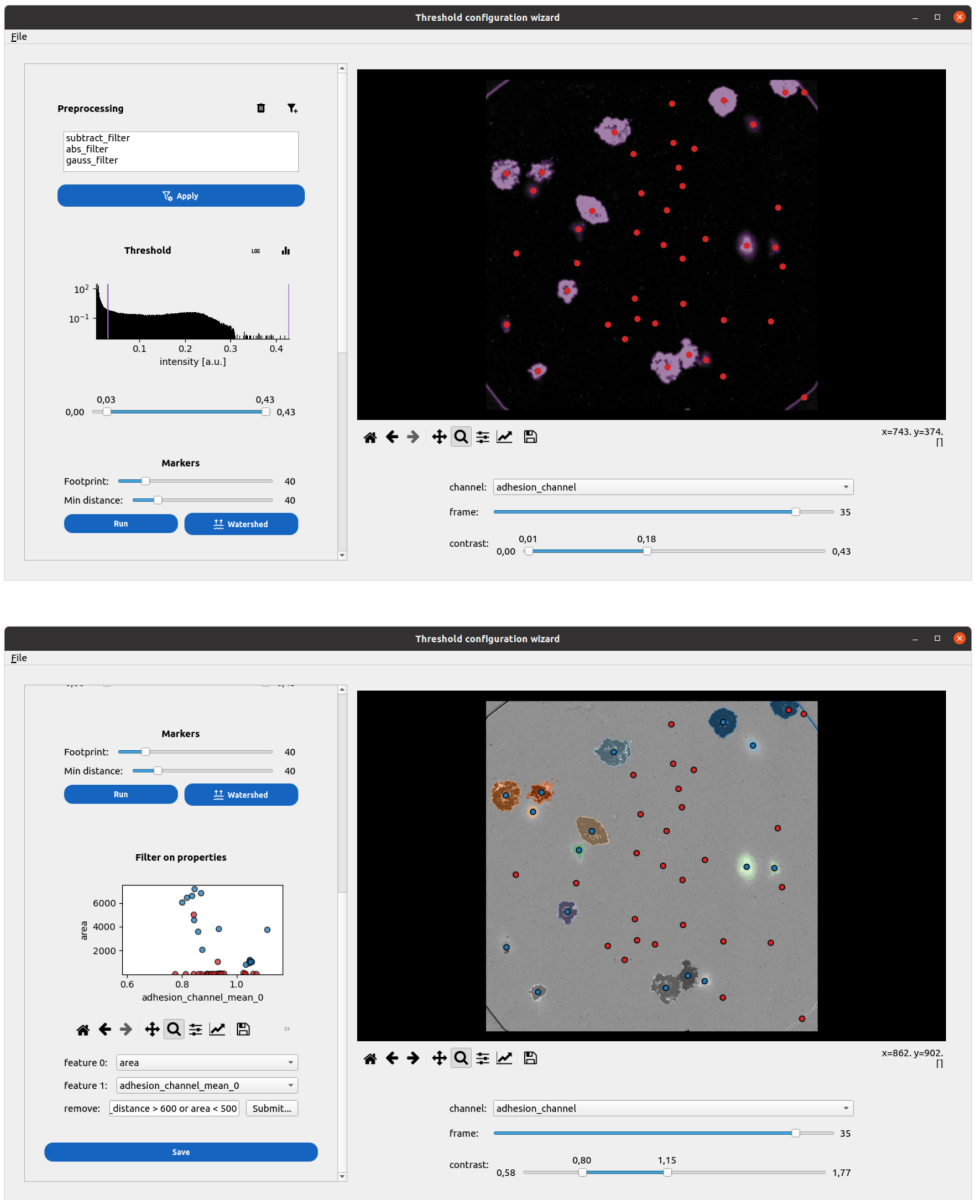

Fig. 8 Interface for segmentation by traditional thresholding with application to RICM images. Top. Selected preprocessing filters are applied followed by manual thresholding using interactive histogram. Bottom: instance segmentation after watershed algorithm and graphical sorting of masks according to selected features measured on the masks (left graph).

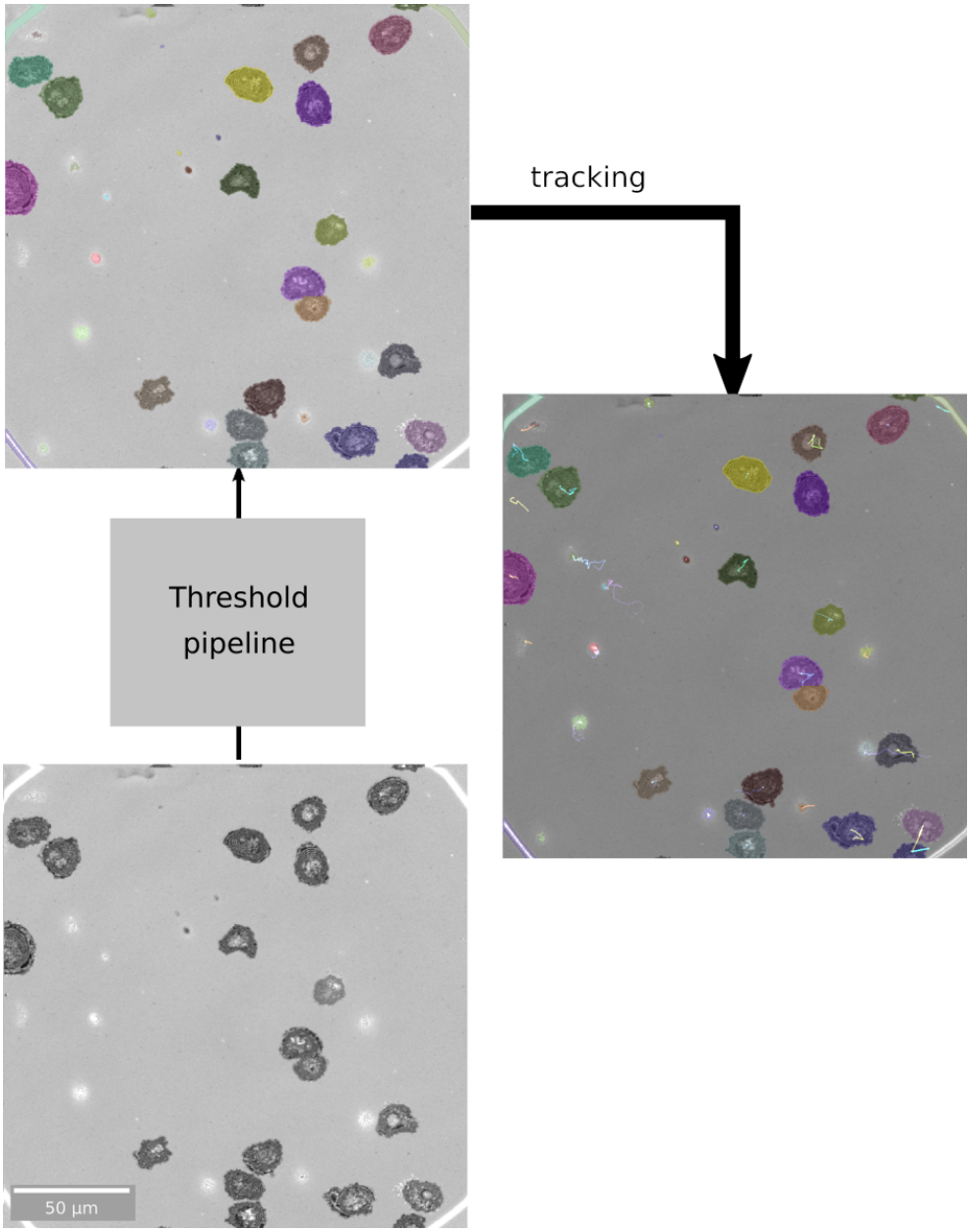

Fig. 9 Cell detection on a normalized RICM image is performed using a traditional segmentation pipeline consisting of a -1 subtraction and absolute value operation, followed by a threshold on the image to detect any cell or object that is different from background. A filter is automatically applied to remove small objects and some false positive detections. The masks are passed to btrack to track all objects before post-track filtering and measurements.

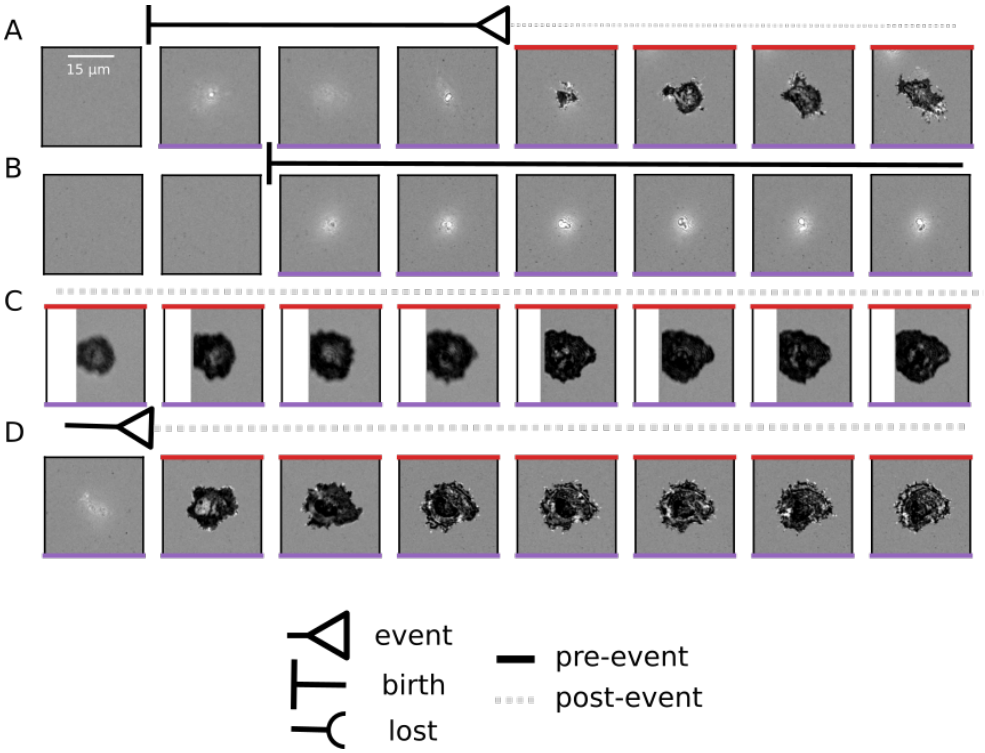

Fig. 10 Hovering duration measurement. A. Hovering duration counted from the first white blob appearance (cell-surface contact) until the first black patch appearance (onset of cell spreading on the surface). B. Hovering without spreading (right censoring). C. Spreading already started at the beginning of the sequence (rejection). D. Contact time not detected (rejection).

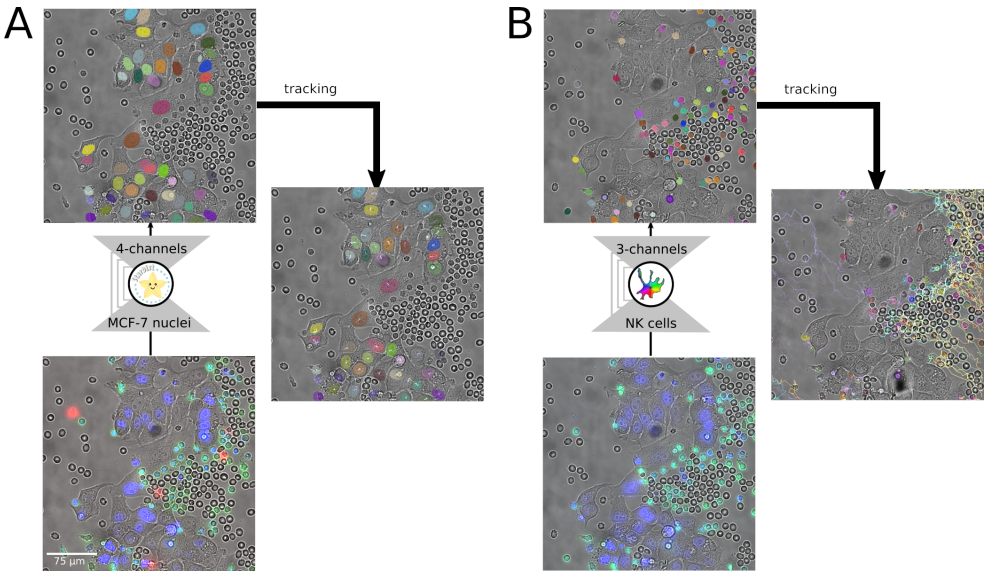

Fig. 11 Pipeline for ADCC analysis. A. A multimodal StarDist model is applied to a four channel ADCC image (brightfield, PI, Hoechst and CFSE) to detect the nuclei of MCF7 cells specifically. The masks are then passed to bTrack for tracking before single cell measurements and signal analysis. B. a multimodal Cellpose is applied to a 3-channel ADCC image (brightfield, CFSE and Hoechst) to segment specifically NK cells among MCF7 and RBCs. The masks are passed to bTrack for tracking, before the single cell measurement step.

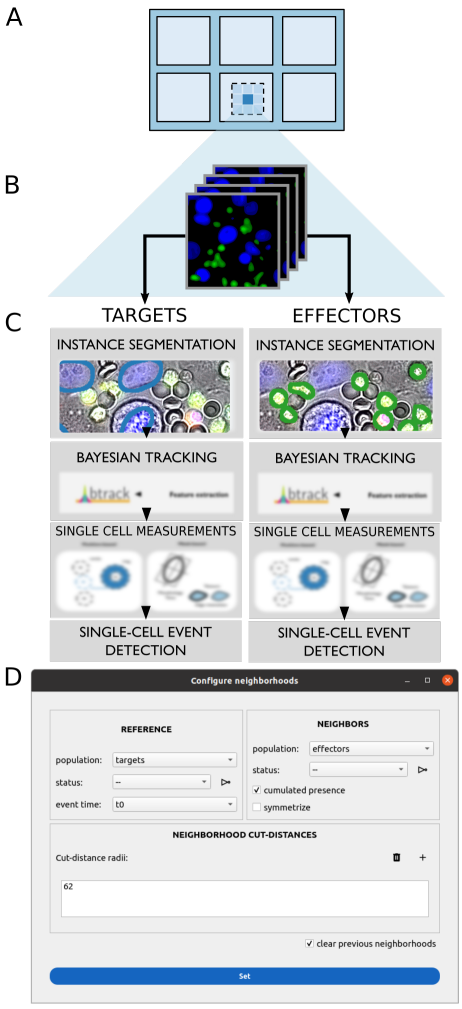

Fig. 12 Two populations analysis pipeline applied to ADCC. A. Multiwell sample. B. 2D multimodal time series. C. Selective segmentation of target cells (left) and effector cells (right), independent tracking of both species, event-detection or annotation, following the pipeline of Fig. 1. D. Software interface for neighbourhood analysis. Choice of reference cell population, status, event time and neighborhood radius list.

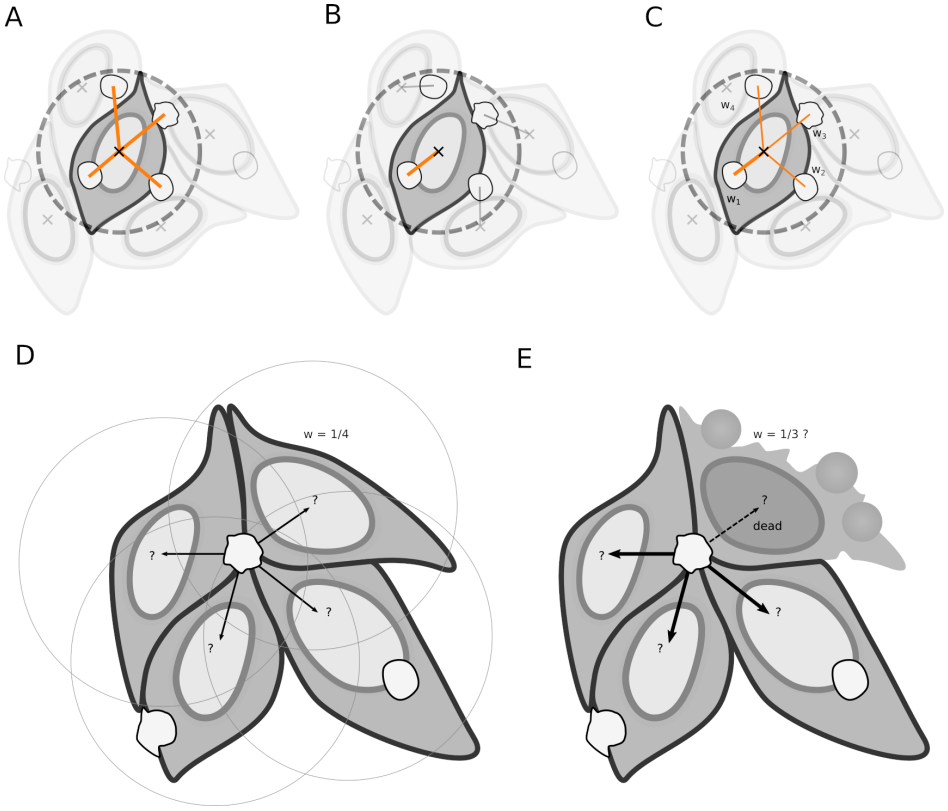

Fig. 13 Proposed neighborhood counting methods. A. Inclusive. B. Exclusive. C. Intermediate. D. the attention weights emerge in the frame of reference of the effector population. An effector may stand at the intersection of many target-centric neighborhoods. The attention weight tries to account both for uncertainty in neighbor attribution and for a potential dilution of the effector activity across the many targets. This weight is attached to the effector in each target neighborhood. Only the intermediate counting method is sensitive to the attention weights. E. In addition, a target that has known an event such as apoptosis may not mobilize an effector cell as much. Therefore, we propose to optionally exclude eventful cells from the attention mechanism.

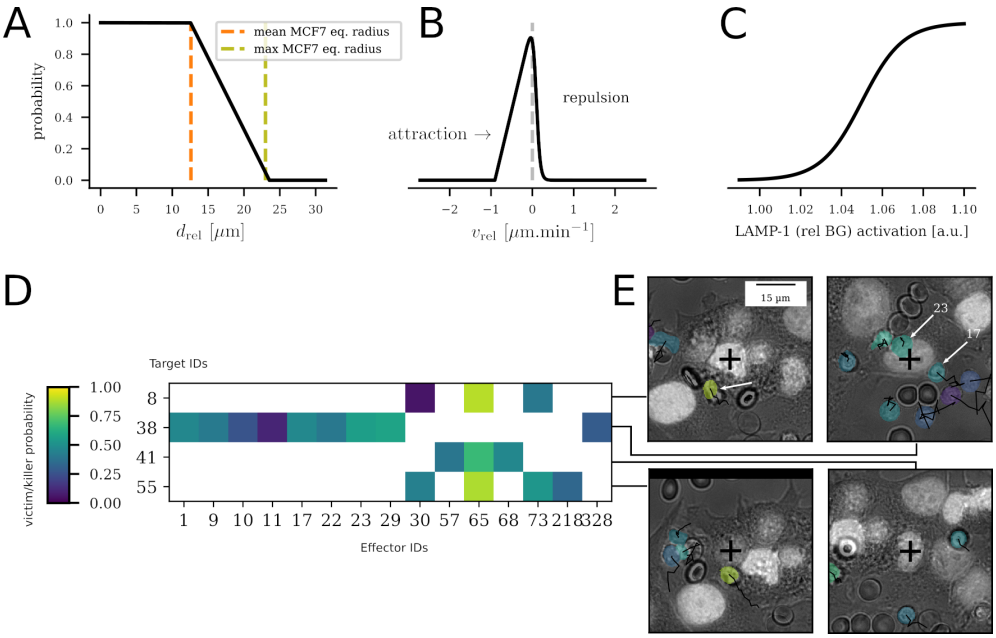

Fig. 14 Killer identification. A-C. Empirical activation functions for determining NK killers. A The mean relative distance between the nucleus of a MCF7 cell and a NK neighbour, in a time window θ_t before the lysis event is mapped to a step-like activation function. For distances smaller than the average MCF7 size, the activation is maximal. Beyond this value, it decreases linearly until the distance reaches the maximum observed MCF7 size. B. The mean relative velocity in the same time window θ_t is mapped to a skewed activation function, favouring low velocities. The instantaneous velocity v_t is computed bidirectionally using a three frames sliding window. The activation function is skewed toward negative values to not penalize NKs getting closer to the target at the time of the lysis event. C. the mean LAMP-1 signal around the time of the lysis event (in a window $\pm\theta_t$) is mapped to a sigmoidal activation function, with a critical LAMP-1 value of 5 % above background. D-E. Optimized probability of a victim/killer pair. D. the matrix shows the optimized probability of having a victim/killer for each target/effector pair in this position. E. Snapshot of the target indicated as a black cross at the center (brightfield and Hoechst in gray, slight CFSE channel in green). The NKs in its neighborhood are recolored to match their probability of being the killer. The probabilities shown here use the following settings and weights: $\theta_t = 15$, threshold=0.400 , $w_v = 0.032$, $w_d = 0.162$, $w_t = 0.374$, $w_I = 0.432$ resulting in $IoU = 0.683$. White arrows indicate the manually annotated most probable killers.

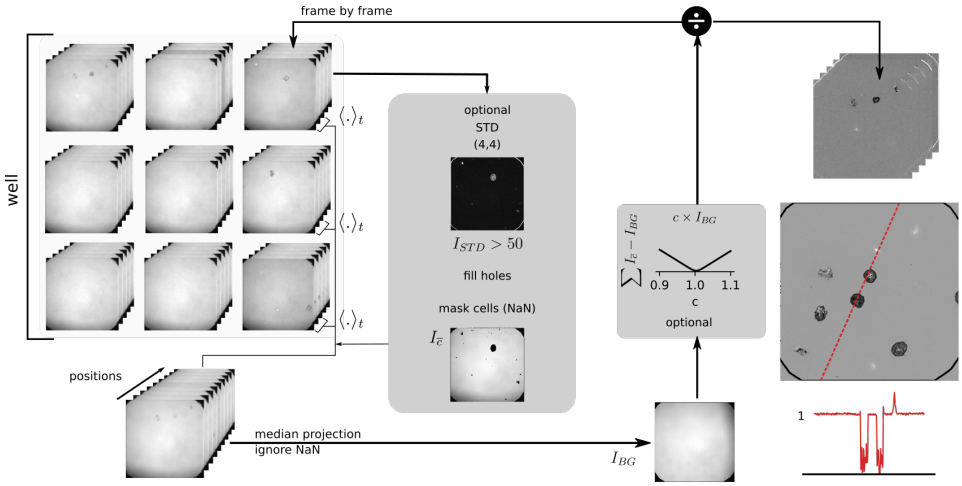

Fig. 15 Workflow for RICM normalization. A background is reconstructed for each experimental condition (well) by using information contained in every single position acquired. The early frames are averaged for each position stacked together. If cells are already visible in those frames, one may want to already mark the cells as "non background". One quick way to achieve this is to perform a rough segmentation with a STD filter and a fill holes operation and mark the cell pixels as NaN. The background can then be reconstructed by performing a median projection of this multi-position stack. Each frame of each position is divided by this background image in order to normalize. Optionally, one can amplify the values of the background to better match with the values of the numerator image, as any loss of focus could change the intensity levels of the original image. A RICM intensity profile on a normalized image shows how spread cells appear darker than the background overall and hovering cells appear brighter.

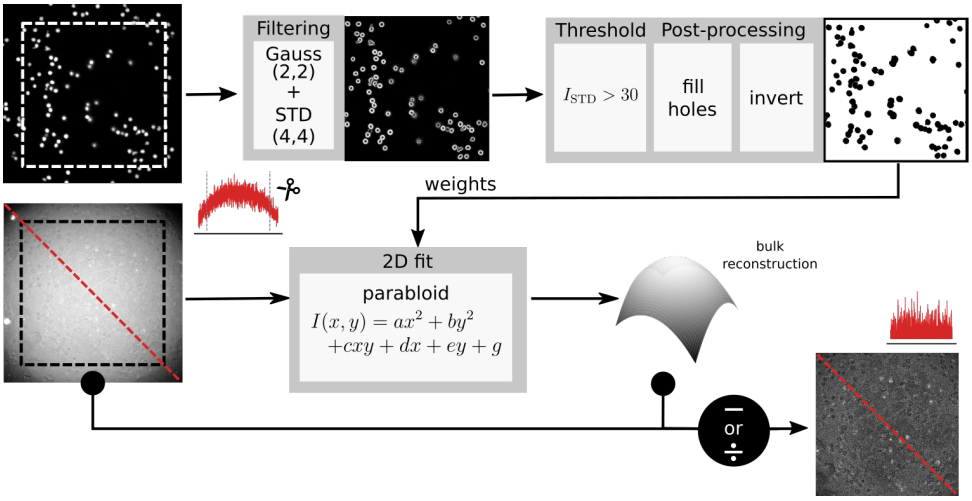

Fig. 16 Workflow for the correction of bulk fluorescence. The fluorescence image is cropped symmetrically along the -x and -y axes to avoid a diaphragm contribution to the intensity distribution. The cells are roughly segmented from the CFSE channel using successively a STD filter (kernel $(4, 4)$), a threshold on the STD transform to binarize the image, a fill holes operation to fill the inside of the detected cell edges and an inversion to set value 0 where the cells are, 1 otherwise. This binary image is used as a weight map to fit the background of the LAMP1 fluorescence image with a 6-parameter paraboloid model. The fitted background is then either subtracted or divided from the raw microscopy image. The process is then reiterated for the next frame.

References

[1] Even-Desrumeaux, K. *et al.* Masked Selection: A Straightforward and Flexible Approach for the Selection of Binders Against Specific Epitopes and Differentially Expressed Proteins by Phage Display. *Molecular & Cellular Proteomics* **13**, 653–665 (2014).

[2] Rozan, C. *et al.* Single-Domain Antibody-Based and Linker-Free Bispecific Antibodies Targeting Fc RIII Induce Potent Antitumor Activity without Recruiting Regulatory T Cells. *Molecular Cancer Therapeutics* **12**, 1481–1491 (2013).

[3] Raynaud, A. *et al.* Anti-NKG2D single domain-based antibodies for the modulation of anti-tumor immune response. *OncoImmunology* **10**, 1854529 (2021).

[4] Gonzalez, C. *et al.* Nanobody-CD16 Catch Bond Reveals NK Cell Mechanosensitivity. *Biophysical Journal* **116**, 1516–1526 (2019).

[5] Limozin, L. & Sengupta, K. Quantitative Reflection Interference Contrast Microscopy (RICM) in Soft Matter and Cell Adhesion. *ChemPhysChem* **10**, 2752–2768 (2009).

[6] Pachitariu, M. & Stringer, C. Cellpose 2.0: How to train your own model. *Nature Methods* **19**, 1634–1641 (2022).

[7] Edlund, C. *et al.* LIVECell—A large-scale dataset for label-free live cell segmentation. *Nature Methods* **18**, 1038–1045 (2021).

[8] Barshir, R. *et al.* The TissueNet database of human tissue protein–protein interactions. *Nucleic Acids Research* **41**, D841–D844 (2013).

[9] Caicedo, J. C. *et al.* Nucleus segmentation across imaging experiments: The 2018 Data Science Bowl. *Nature Methods* **16**, 1247–1253 (2019).

[10] Kumar, N. *et al.* A Multi-Organ Nucleus Segmentation Challenge. *IEEE Transactions on Medical Imaging* **39**, 1380–1391 (2020).

[11] Naylor, P., Lae, M., Reyal, F. & Walter, T. Segmentation of Nuclei in Histopathology Images by Deep Regression of the Distance Map. *IEEE Transactions on Medical Imaging* **38**, 448–459 (2019).